Pergamon

Int. J. Solids Structures Vol. 32, No. 8/9, pp. 1017–1046, 1995

0020-7683/95 $9.50 + .00

0020-7683(94)00188-X

AXIAL PERFORATION OF ALUMINUM HONEYCOMBS BY PROJECTILES

WERNER GOLDSMITH and DELL L. LOUIE
Department of Mechanical Engineering, University of California, Berkeley, CA 94720, U.S.A.

(*Received* 31 *June* 1994; *in revised form* 28 *July* 1994)

Abstract—Deformation and energy absorption characteristics of aluminum honeycomb when penetrated or perforated in the axial direction by spheres and cylinders with diameters of the order of and twice the cell size have been observed experimentally. The work of static penetration using a standard test machine was obtained from measured force histories when hard-steel spheres with three different diameters were pushed through the sample. Ballistic impact was accomplished using a compressed gas gun by projecting these spheres and a blunt cylinder against the target at normal incidence over the velocity range 30–183 m/s (100–600 ft/s). Embedment corresponding to the ballistic limit was achieved for the slowest projectiles; at slightly greater initial speeds, the strikers exited with residual velocities that were measured.

In static perforation, deformation mechanisms were strongly influenced by the location of contact when the cell size approximated the sphere diameter, resulting in substantial variations in the absorbed energy. When initial contact occurred at the center of the cell, the walls would bend and often tear and delaminate. When contact initiated at a cell wall, the deformation resulted from either out-of-plane or in-plane crushing throughout the entire sample, or else axial crushing to a certain depth with a subsequent transition to in-plane crushing in addition to wall fracture and delamination. When the penetrator diameter was substantially larger than the cell size, the initial contact location was less critical; the deformation pattern consisted of either in-plane or out-of-plane crushing, or a combination of the two. Out-of-plane crushing, which sometimes produced a plug, was found to require a greater amount of energy to achieve perforation.

Similar damage patterns were observed in the ballistic tests involving two sizes of spheres. By contrast, the cylindrical striker, whose diameter was either equal to or greater than the cell size, always produced axial crushing and generated a plug. Ballistic limits were obtained for 10 combinations of honeycomb samples and projectiles; a wider spread for identical initial conditions was obtained compared to homogeneous targets that is also due to the slight variability of the original contact position. As expected *a priori*, for a given target geometry, higher ballistic limits were found for smaller masses and/or larger projected areas; conversely, for a particular projectile, the honeycomb with a thicker foil and/or smaller cell size exhibited the higher limit.

The work performed in the perforation process could not be properly predicted by a simple analysis based solely on energy considerations for in-plane and out-of-plane crushing, although a greater fraction of the total perforation energy was calculated when the latter damage pattern predominated. A substantial or often preponderant amount of energy is consumed in random tearing and delamination of the walls that cannot be quantified because their occurrence and extent cannot be predicted or even precisely measured at the present time. These fractures are random due to the sample manufacturing process as well as the precise position of initial contact with the cellular geometry, documenting the dominant influence of the microstructure. However, if the measured ballistic limit is regarded as a system property—as is generally the accepted practice—predictions of the terminal velocities based on this value were found to be in good agreement with the measurements.

INTRODUCTION

Honeycombs constitute the crucial core segment of sandwich components that are used in numerous structural applications as well as for energy absorption purposes. They are primarily manufactured as sheets (although they have been used for shells on occasions) consisting of adjoining thin-walled tubular cells whose axes are normal to the plane of the layer, composed of aluminum, paper covered by a polymeric fluid, or Kevlar– or graphite–epoxy composites. The cells vary in cross-sectional shape and dimensions as well as wall thickness. The cores comprise a "composite" material featuring single or bonded dual walls enclosing empty space. Their attributes include low unit weight with constant axial crush strength as well as substantial shearing resistance in directions parallel and perpendicular to the cell axes, while the facings of the sandwich carry bending loads. The geometric features and mechanical properties of the core play a major role in delineating the loading

capacity and energy absorption capability of the sandwich structure [see e.g. Gibson and Ashby (1988); Zhang and Ashby (1989); Goldsmith and Sackman (1992); Moriarty and Goldsmith (1993); Jamjian *et al.* (1994)].

Another important feature of the sandwich plate is its penetrability, particularly in space applications or when the unit is used for protective purposes. Here, also, the behavior of the core will be of importance in determining the perforation resistance of the composite. Quantitative data on this subject and an understanding of the deformation characteristics of the honeycomb are currently not available, but are needed by both manufacturers and their customers as a first step in obtaining the corresponding information about the sandwich (currently under study). The penetration response is expected to be quite different for the honeycomb, whenever the diameter of the indenter is of the order of or slightly larger than the cell size, than for a more homogeneous structural element such as a metallic or plastic plate. Furthermore, a much wider spread of the data is to be expected for cellular objects due to the dominant influence of the microstructure. As the diameter of the penetrator increases for a fixed cell dimension, the macroscopic response of the honeycomb will more closely approach that of a homogeneous material, although differences due to anisotropy will still exist.

The present work is an initial study of the phenomena manifested in the axial penetration and perforation of honeycombs by small objects, selected here as spheres or cylinders with diameters comparable to or twice that of the cell. This was performed under both static and ballistic loading conditions using a standard testing machine or a gun-launched projectile, respectively. A variety of deformation and failure mechanisms were observed for both types of loading. The energy absorbed in the penetration or perforation was computed from statically determined force–displacement histories and from the impact and exit velocities (when present) for the dynamic tests; the ballistic limit† was also determined from these data, occasionally by interpolation.

EXPERIMENTAL ARRANGEMENT

(1) *Static penetration*

Quasi-static loading of samples was produced by the action of a standard Instron testing device (either Model 1331 or Floor Model TT-C) with motion produced by the lower ram or upper crosshead, respectively. The indenter was rigidly attached to the bottom surface of the upper member by means of a connector of smaller diameter, while the sample was positioned horizontally in a mount located on top of the lower platform of the machine. A set-up where samples were clamped only along two edges proved to be unacceptable because the specimens buckled under load rather than experiencing penetration. In consequence, a different, very stiff mount was designed where the sample was the core of a sandwich with a bottom 152 mm square steel plate, 6.35 mm thick, fastened to two sections of Unistrut, and a top facing of plastic, 2.8 mm thick, all clamped together. A concentric hole of 15.88 m diameter in the cover plates allowed perforation at constant speeds of either 0.0762 or 0.127 mm/s; the size of this opening will make some difference in the deformation of the honeycomb immediately outside the area penetrated. However, it is very likely that the effect of this constraint is reduced under dynamic conditions and the effect of its size was not further investigated. Instron load cells of 10 and 4.45 kN capacity for the two test devices, respectively, registered the force histories on a strip recorder and on a digital oscilloscope.

Three sphere sizes with diameters of 3.56 mm, 6.35 mm and 12.7 mm were employed as penetrators; these were cemented with epoxy to the appropriately contoured end of 25.4 mm long cylindrical steel rods with diameters slightly smaller than the spheres. The other end of the rods protruded from a rectangular block with a tapped hole permitting bolting to the upper portion of the testing machine.

† The ballistic limit, v_{50}, is a statistical value denoting the average initial speed of a completely specified projectile/target geometry and material so that 50% of the strikers just pass through the object. However, various definitions of what constitutes such a perforation exist and are subject to interpretation by the beholder (see e.g. Backman and Goldman, 1978).

(2) *Ballistic tests*

Axial impact tests on honeycomb plates mounted in a target holder were executed by means of a pneumatic gun with three interchangeable barrels of 3.89, 6.43 and 12.9 mm diameter, each 1.37 m long; this unit, similar to that described by Liss and Goldsmith (1984), was rigidly supported by a heavy steel table. The experimental arrangement is depicted in Fig. 1. A detachable compressed air reservoir permitted insertion of the projectile into the breech end of the barrel where it was restrained by a protruding pin which was retracted for firing. Parallel beams from two minilights, 152 mm apart passing through two slits on opposite sides of the barrel were focussed on two minilights; their interruption by projectile passage produced signals on an oscilloscope that provided the initial velocity. Two cardboard screens painted with a silver grid, each attached serially to a voltage source and an oscilloscope, acted as open circuits until closed by impingement of the projectile; the resulting signal permitted the evaluation of the terminal velocity. The position of the holes in these screens also indicated that any deviation of the initial trajectory was negligible.

The honeycombs were positioned vertically in a holder so that their axes were parallel to the striker trajectory. Unlike the static case, the sample, in most cases, was clamped at two opposite edges. However, for the largest projectiles, a fully clamped configuration was devised similar to that for the static tests, with holes of 15.88 mm diameter drilled through the facings to ensure unimpeded projectile passage. These support arrangements were found to produce negligible global deformation of the entire sample, in this respect simulating the set-up for static perforation.

The projectiles consisted of steel spheres with a Rockwell hardness of R_C 60–63 and diameters of 3.56 mm, 6.32 mm (0.25 in), and 12.7 mm (0.5 in) as well as a blunt hard-steel

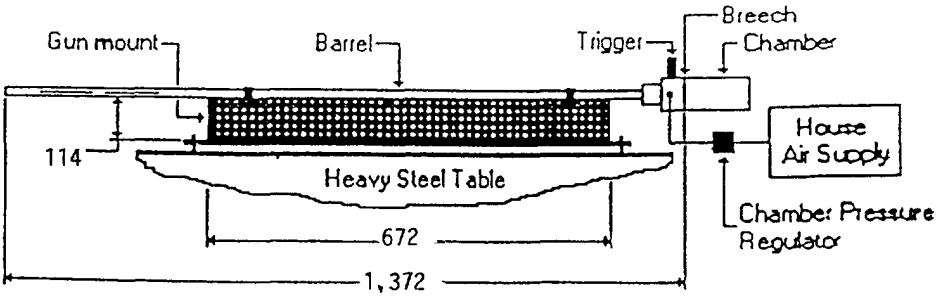

Gun and Support

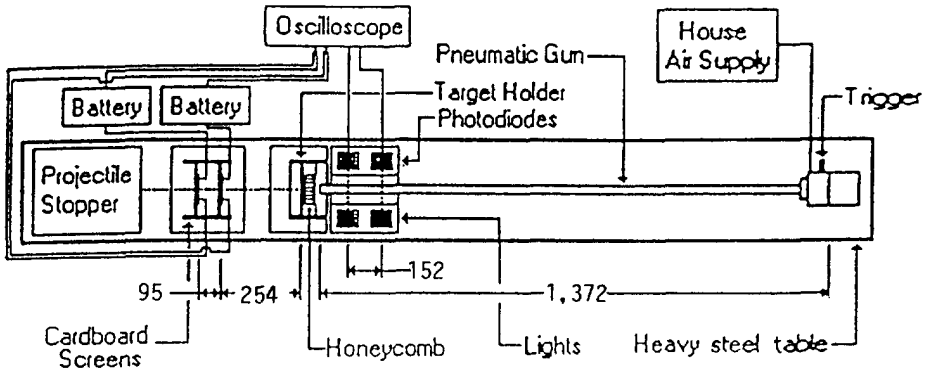

Experimental Arrangement

Fig. 1. Schematic of experimental arrangement.

Table 1. Mechanical properties of 5052 H19 aluminum sheet

Property	Foil thickness 0.025 mm	0.051 mm
Density (kg/m^3)	2678	2678
Young's Modulus, E (GPa)	71	71
Poisson's ratio,	0.33	0.33
Tensile Yield Strength (MPa)	255†	255†
Ultimate Tensile Strength (MPa)	290	290

Honeycomb designation	Density (kg/m^3)	Static crush strength, kPa Hexcel	Measured
1/8-5052-.001	72.1	1793	—
1/8-5052-.002	129.7	5171	4916
1/4-5052-.001	36.8	517	558
1/4-5052-.002	66.9	1586	1606

† Estimated from 5052 H19 aluminum alloy.

cylinder of 6.32 mm diameter and 19.07 mm (0.75 in) length. The masses of the bullets were 0.186, 1.04, 8.35 and 4.66 g, respectively. A striker catcher was placed beyond the terminal velocity screens; it consisted of a plywood box filled with wood, cardboard and foam.

The four classes of hexagonal honeycombs used here consisted of 5052 H39 aluminum foil with a cell width of 3.175 mm (1/8 in) for two types and 6.35 mm (0.25 in) for two others. A wall thickness of 0.0254 (0.001 in) and of 0.508 (0.002 in) was used in conjunction with each cell diameter; all samples were 19.05 mm (0.75 in) thick. The manufacturer labeled the specimens as 1/8-5032-.001, 1/8-5052-.002, 1/4-5052-.001, and 1/4-5052-.002, respectively, denoting cell size, material and wall thickness†. While the material was initially in the H19 state, the cold work and heat treatment transformed the foil effectively into 5052 H39 aluminum whose properties are not documented. In consequence, the present work relies upon the available data for the H19 state. The mechanical properties of this material and the crush strengths of the honeycombs, provided by Hexcel Corporation (1988) are listed in Table 1.

DATA ANALYSIS

(1) *Static tests*

Digital information from the Instron Model 1331 produced load histories of roughly trapezoidal shape with superposed oscillations of about 0.2 Hz, not present in the strip chart recorders and attributed to mechanical and electrical noise in the load cell, that were eliminated by use of a Fourier transform program. Zero load adjustment was achieved by subtracting the weight of the indenter and its mount as well as associated machine hardware.

A linear calibration process converted the voltage history to a loading history or, alternatively, a load–displacement curve. A typical strip chart test result for a 1/8-5052-.002 aluminum honeycomb, 19.05 mm thick, penetrated by a 3.56 mm (0.14 in) diameter steel sphere—of nearly the same size as the cell diameter—is shown in Fig. 2. In this run, the sphere touched initially at the cell center; the work performed in this test was determined from the area under the curve that represented the work of perforation, 1.544 J.

(2) *Ballistic tests*

In view of minimal barrel friction and venting of the back pressure by the slits in the barrel, the assumption that the measured initial projectile velocity represents its exit speed from the barrel is considered excellent. A correction in the terminal velocity was incorporated by including the speed reduction produced by the tearing of the first screen, calibrated by target removal and comparison of the initial speed measurement using the

† Hexcel Corp., Dublin, CA.

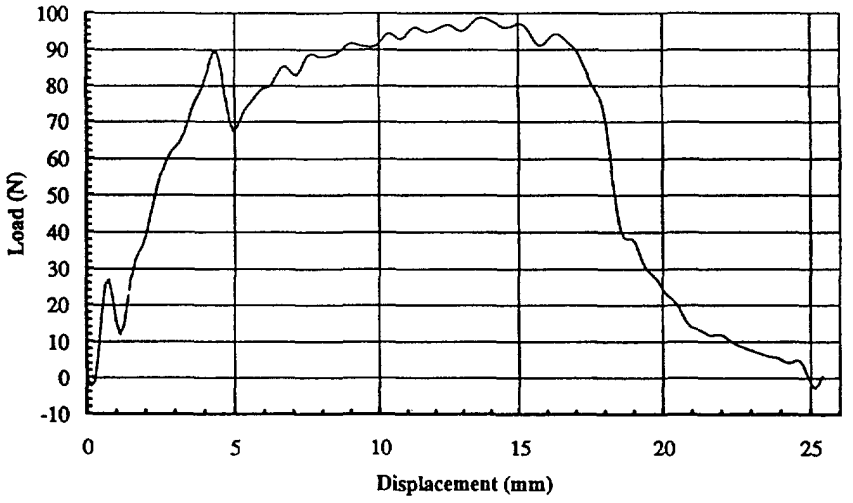

Fig. 2. Static load history for the penetration of a 1/8-5052-.002 aluminum honeycomb 19.05 mm thick by a 3.556 mm diameter steel sphere at a speed of 0.127 mm/s. Perforation Work: 1.544 J.

minilights with the uncorrected value obtained from tearing of the paper screens; the last data were projectile shape and mass dependent.

The ballistic limit for each geometric arrangement was chosen as the average of the highest velocity that did not and the lowest value that did produce perforation. Except near or below this limiting value, the initial contact point of the striker had a substantially smaller or even a negligible effect on both the damage patterns (which were fewer in number) and hence the work of perforation compared with that involved in the quasi-static penetration tests.

RESULTS AND DISCUSSION

(1) *Damage processes*

The observed deformation characteristics of the honeycombs resulting from penetration are unique and exclusively due to their cellular nature; they are not sufficiently well understood at the present time to permit accurate analytical modeling. They differ almost completely from those described in the literature for homogeneous materials such as solid plates of metal under corresponding conditions. For *uniform* targets, damage has been observed and analytically depicted as occurring by (a) hole enlargement [see e.g. Taylor (1948), Thomsen (1955)]; (b) petalling [Landkof and Goldsmith (1985)] where initial crack propagation is followed by bending of the separated strip; (c) the process of plugging, with shear playing a dominant role [see e.g. Recht and Ipson (1963); Liss *et al.* (1983); Liss and Goldsmith (1984)], and (d) the previously cited global target deformation involving plate bending [see e.g. Jenq and Goldsmith (1988)].

In the present experiments, the mounting of the sample permitted neglect of any work done in producing global deformation. The destructive patterns that were observed for the honeycomb plate included out-of-plane (axial) crushing [see e.g. Wierzbicki (1983); Zhang and Ashby (1992a)]; in-plane crushing, which may occur subsequent to out-of-plane crushing when a sphere of similar diameter to that of the cell slips into the cell center; plastic bending of the cell walls, sometimes repeatedly, that is not part of crushing; tearing of multiple cell walls, whose extent was frequently difficult to determine; and delamination of the cell walls. Under certain circumstances, a plug is generated, often attached in case of static perforation; this phenomenon invariably occurred in dynamic tests with the blunt-faced striker when its diameter is greater than the cell size and nearly always so when of the same size. However, this situation has also been found under some static conditions. Cell enlargement as the only major damage mechanism takes place only when the penetrator has a diameter approximating that of the cell and is placed at the cell center; it is manifested by a single bending of the cell walls with, at most, minor tearing of the material.

(*a*) *Out-of-plane* (*axial*) *compression*. The major mechanism of out-of-plane compression is depicted in Fig. 3(a) when the penetrator whose diameter matches that of the cell is positioned over a single cell wall of thickness h. Here, the ultimate compressive strength of the walls is exceeded, leading to crushing of the material directly below and tearing of portions of the adjoining four walls by a combination of plastic deformation, fracture and delamination at the locations indicated. The result is manifested by an accordion-type collapse which, when fully implemented (densification) will generate a plug during subsequent motion. Wierzbicki (1983) has shown that this crushing occurs at a constant stress level or, alternatively, under nearly constant load when specimens are rigidly backed, until the core has been completely densified which occurs somewhere between 75% [Zhang and Ashby (1989)] and 84% [Goldsmith and Sackman (1992)] of the original thickness. Such compaction was occasionally found in the static tests, but transpired invariably in dynamic loading when the cylindrical projectile was employed. Based on the results of Wierzbicki (1983), the crushing component of the out-of-plane work, W_{oc}, for a circular projected penetrator area of diameter D and crush depth to densification of $0.75b$ (with b as the layer thickness), can be approximated by the expression

$$W_{oc} = 9.75\, S_y b D^2 (h/s)^{5/3} \tag{1}$$

where S_y is the flow stress and s and h are the cell size and wall thickness.

Microscopic examination of a number of fracture surfaces indicate necking and hence a tensile deformation and failure, demonstrated by ductile surface craters. When this happens near the junction of the walls, delamination of the double-walled segment to some extent is also likely to occur. Thus, while the work of axial crushing can be obtained from eqn (1), the fracture and separation of the walls are not included in the total energy dissipation. These last two features constitute an extremely complicated process of damage generation that probably represents the preponderant portion of the penetration work. As an example of the uncertainty involved here, based on a shear strength of 174 MPa for aluminum, the shearing of four walls each 0.025 mm (1 mil) thick for one-half of the panel thickness alone requires about 3 J of energy, which corresponds to the maximum perforation energy required here in any of the static or dynamic tests.

When the penetrator diameter is twice that of the cell size, the walls in front of the indenter will be crushed axially, while the six walls connecting the crushed and uncrushed regions are plastically deformed, as shown in Fig. 3(b). The crushing component of the perforation energy is still given by eqn (1). While a number of models have been presented that depict the axial crushing of a single tube, no analysis currently exists for the elasto–plastic deformation of a connected network of cells as is present in a honeycomb.

(*b*) *In-plane* (*lateral*) *crushing*. Perforation also subjects the honeycomb to loads normal to the cell axes (in-plane-loading), where the wall bends elastically until crushing eventuates due to a combination of elastic buckling and plastic collapse [see e.g. Klintworth and Stronge (1988, 1989); Zhang and Ashby (1992b)]. As this process continues, the stress gradually decreases to a constant level, the in-plane crush strength, that can be determined by a plastic collapse analysis; it is lower than the out-of-plane crush strength.

A variety of damage characteristics exist for this mode depending on contact and tearing locations; two typical patterns observed in the tests are shown in Figs 4(a) and 4(b). The first case corresponds to Fig. 3(a) where placement occurs at the center of a single layered wall (but the penetrator diameter approximates the cell size), while the penetrator diameter here is double this size. For the situation depicted in Fig. 4(a), the indenter tears the two adjoining walls that are then rotated 30° about their plastic hinges, representing the minimum angle for unobstructed passage. Concurrently, the indenter crushes the single-layered wall and the other two adjoining walls in the direction of the straight arrow. This process, including tearing and bending of the cell sides, produces the necessary space for perforation, as exemplified for a ballistic test by Fig. 5. This photograph clearly depicts the

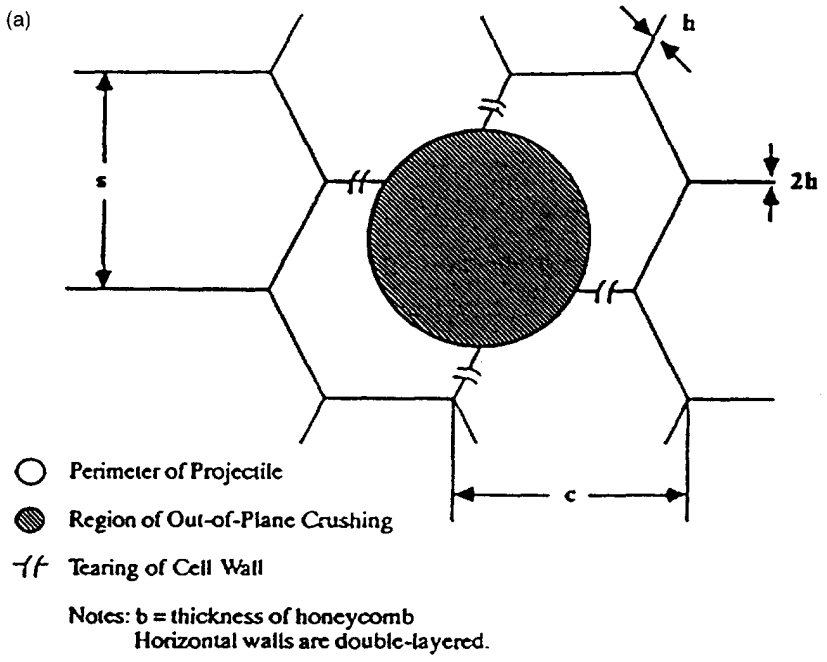

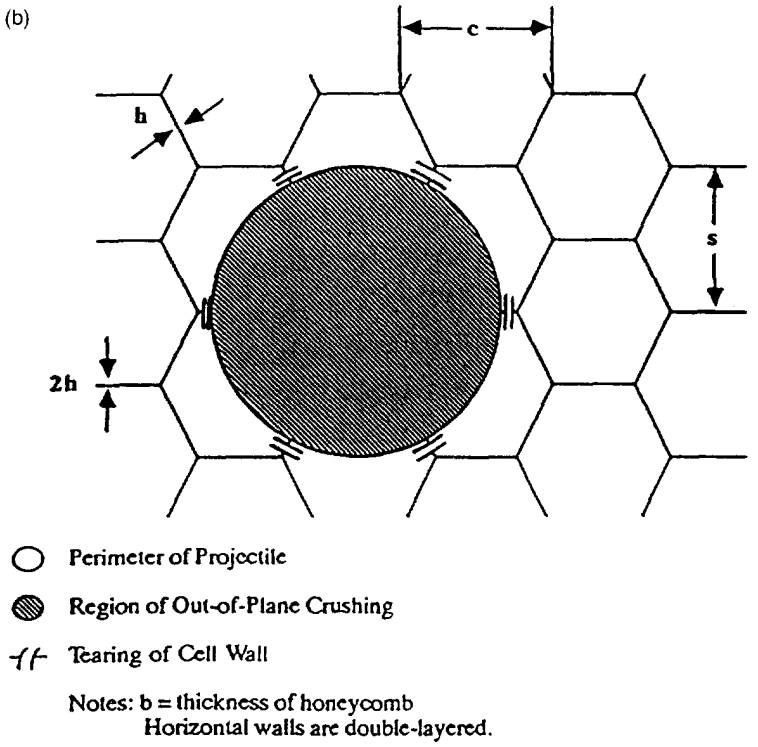

Fig. 3. Deformation from out-of-plane crushing for an indenter with a diameter (a) approximately equal to the cell size placed over a cell wall (b) approximately equal to twice the cell size.

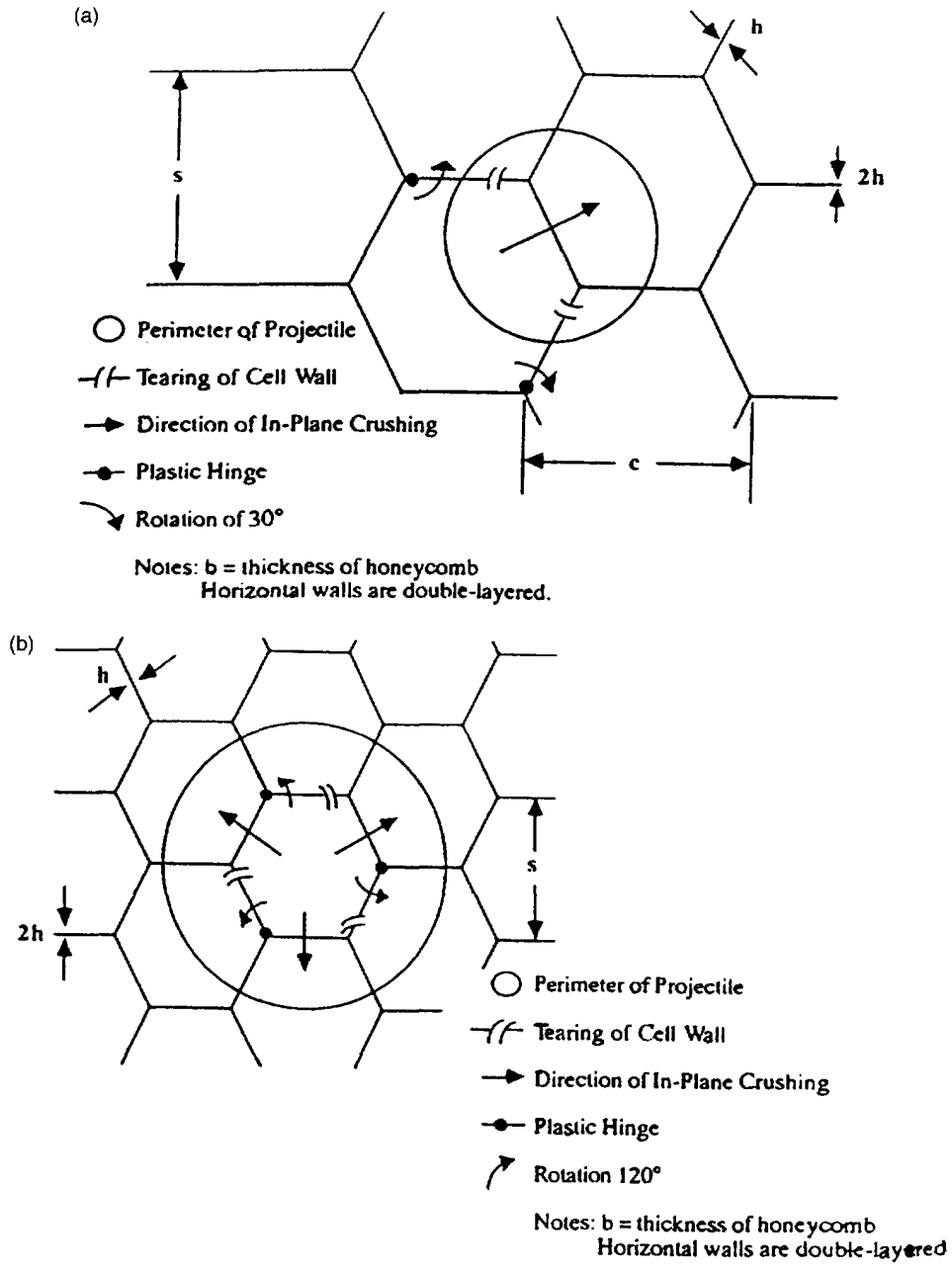

Fig. 4. Deformation from in-plane crushing for an indenter with a diameter (a) approximately equal to the cell size placed over a cell wall (b) approximately equal to twice the cell size.

tearing and in-plane crushing processes involving lateral displacement of three sides of an original hexagonal element into the corresponding walls of the adjacent cell.

The work for this mode of perforation, W_{ic}, results from bending, in-plane crushing, tearing and delamination. The first two processes have been quantified to provide the expression [Louie (1992)]

$$W_{ic} = 2.96\, S_y b h^2 \tag{2}$$

which, as in the case of eqn (1), also fails to include the dominant dissipation mechanisms of tearing and delamination.

The special type of in-plane deformation comprising essentially only cellular derangement requires only the specification of the two geometric conditions for the size and initial

contact point of the penetrator; it is very reproducible. However, tearing and delamination processes may vary considerably due to even slight differences in manufacturing practices and also due to the effect of variations in the contact position. Nevertheless, the data obtained here are consistent and permit an accurate determination of the energy absorbed in penetration and hence, for dynamic loading, the value of the ballistic limit, v_{50}. The concomitant exit velocity, v_f, for higher initial speeds, v_0, is then obtained from Recht and Ipson's (1963) expression

$$v_f^2 = \frac{1}{2}\frac{m}{m+m_p}(v_0^2 - v_{50}^2) \tag{3}$$

where m is the mass of the projectile and m_p is the mass of the plug or displaced material, assumed to travel at the same final speed as the striker.

The critical effect of initial location of the penetrator on damage mechanisms and, hence, on the work of perforation is shown by a comparison of Figs 6 and 7. Both relate to the static perforation of a 1/8-5052-.001, 1905 mm thick sample, by a sphere of 3.556 mm diameter, just slightly larger than the cell size. In Fig. 6, the initial contact point was a cell wall which required penetration work of 0.556 J, primarily due to axial deformation and the production of a plug. In contrast, in Fig. 7, the sphere was originally positioned at or near a cell center, so that its indentation generated only bending and some tearing of the cell walls without either significant in-plane or out-of-plane deformation; the work of perforation was found to be 0.256 J, approximately 46% of the value for the previous case.

(2) *Static penetration tests*

Each of the four types of 5052 aluminum hexagonal honeycombs (1/8-.001, 1/8-.002, 1/4-.001 and 1/4-.002) was perforated in six repeated tests under as identical conditions as could be reasonably produced experimentally by two spheres with diameters equal to the nominal size and twice that of the cells. In general, for all samples and penetrators, the damage pattern consisted of in-plane and/or out-of-plane crushing, plastic bending of the cell walls independent of crushing, delamination as well as tearing of either two or four of the walls, and, under certain conditions, the formation of a plug. For spheres with the same diameter as the cell, the slower indentation speed generally requires greater energy to produce perforation.

As stated repeatedly, initial placement of the penetrator is critical; when the sphere is originally positioned in the center of the cell, its enlargement ensues by plastic in-plane deformation, with relatively little energy expenditure. When the sphere first touches a wall or the junction of cells, these walls crush axially, while the walls at the boundary of this region bend plastically, delaminate and tear requiring substantially greater energy dissipation. Lateral shifting of the sphere to the cell center may occur at any stage in which case axial crushing is transformed into transverse deformation mechanisms requiring smaller amounts of energy.

If two of the four walls at the sphere perimeter tear, axial crushing can no longer be produced. Instead, the sphere rotates the damaged material 90° and pushes it into the surrounding honeycomb, with the intact walls providing the necessary hinge action. Upon removal of the damaged aluminum, a sudden drop in resistance manifests the transition from axial to in-plane crushing of walls that continues until perforation is complete.

When all four walls tear, the aluminum is not displaced sideways, and thus the sphere continues its axial crushing with plastic bending delamination and tearing of the walls joining the crushed and undamaged regions. Near perforation, these walls can no longer support the axial crush load, the walls bend and tear and a plug is formed, which may remain attached to the target as shown in Fig. 6.

(*a*) 3.175 *mm* (1/8 *in*) *cell size*. The load records for the three types of primary damage generation are illustrated in Fig. 8 for the 1/8-.001 specimens penetrated by the 3.56 mm sphere. The oscillations present, particularly for Run 44, where out-of-plane crushing

occurred for a depth of 14.5 mm before in-plane crushing initiated, are the result of folding of the cell walls, similar to that found by Goldsmith and Sackman (1992). The pattern of Run 44 corresponds to the force curve that produced the damage shown in Fig. 6, while that of Run 21, with initial sphere placement at the cell center, is similar to the force–displacement relation that generated the cell enlargement typified by Fig. 7.

A second series of six tests was performed on this honeycomb with a 6.35 mm diameter sphere, double the size of the cell. Here, the initial placement was not as critical, and primary damage solely from cell enlargement cannot occur. The lowest energy required was manifested in two of the runs, with perforation energies of 0.708 and 0.811 J, respectively, where out-of-plane crushing was either absent or present for only a small amount of penetration (about $\frac{1}{10}$th the thickness). The remaining tests exhibited significant initial out-of-plane crushing for distances ranging from 13.4–17.3 mm and terminal plug formation, resulting in an average of double the amount of energy (1.28–1.48 J) required for perforation under primarily in-plane crushing conditions.

A parallel set of six tests for each of the two spheres was conducted on the 1/8-.002 honeycomb where the target exhibited twice the wall thickness of the previous series. Here, initial location for the smaller sphere is even more critical; an original central position or early displacement to the cell center and penetrating by bending and tearing of cell walls again requires much less energy for perforation, about 1.36–1.54 J. Increased presence of axial crushing together with wall bending, tearing and delamination and, even more potently, plug generation required successively larger quantities of energy. However, the highest amount of work applied, 2.27 J, occurred for a unique case where the sphere migrated to the cell center and plastically bent the walls without any tearing or delamination, indicating the enormous potential for dissipation by the mechanism of plastic bending of metal sheets.

Three of the runs employing the 6.35 mm diameter sphere featured axial crushing ahead of the penetrator, while the walls at the perimeter bent, tore and delaminated; at a certain depth, about 13.2 mm, crushing ceased and a plug was formed. The force–displacement curves are trapezoidal with a gradual rise over 3 mm of displacement, a plateau of about 250 N for a distance of 11.5 mm and a gentle decay up to perforation, requiring a total energy of about 3.5 J.

The other three runs also exhibited initial axial crush as indicated by a gradual rise of the force; however, at various penetration depths, ranging from 6.8 to 13.2 mm, the load decreased abruptly, indicating a change of mechanism to in-plane compression without plug formation. From the previous observations, it might be presumed that the latter tests would require less work of perforation than the initial three; however, the opposite is the case. The last three runs exhibited more triangular-shaped force–indentation curves with higher peak and average force levels of 360 N and 260 N, respectively. One possible explanation is some suppression of the wall tearing process that resulted in greater load carrying capacity of the crater perimeter while ripping provided an opening for perforation by in-plane crushing. This is illustrated in the normal and sectional views for Run 40 shown in Fig. 9 with the path of the penetrator from left to right. The transition from axial to transverse crushing is clearly evident; further, it is seen that the axially crushed region has been folded over by 90° and pushed into the honeycomb.

(*b*) 6.35 *mm* (1/4 *in*) *cell size*. Again, six tests were performed with 6.35 mm steel sphere penetrators on samples with 0.001 in (0.025 mm) wall thickness. The damage pattern in four of the runs corresponds identically to the first combination of 1/8-.001 5052 aluminum cells indented by a 3.175 mm (1/8 in) diameter ball. As exemplified by Fig. 10 (Run 9), this began with axial crushing consisting of plastic bending, delamination and wall tearing, as manifested by the initial rise for 5.08 mm, until the sphere slipped to the cell center initiating in-plane crushing, with corresponding load diminution, completing the perforation by bending and tearing of walls to provide a perforation energy of 0.429 J. The depth of transition to in-plane crushing for these runs was remarkably constant, ranging from 5.08–5.59 mm for four of the six runs and involved perforation energies varying from 0.264 to 0.454 J; these variations are attributable to the tearing and delamination of a different

Fig. 5. Damage pattern produced by in-plane crushing in the perforation of a 1/4-.001 5052 aluminum honeycomb 19.05 mm thick by a 6.35 mm (1/4 in) diameter steel sphere at a velocity of 152 m/s.

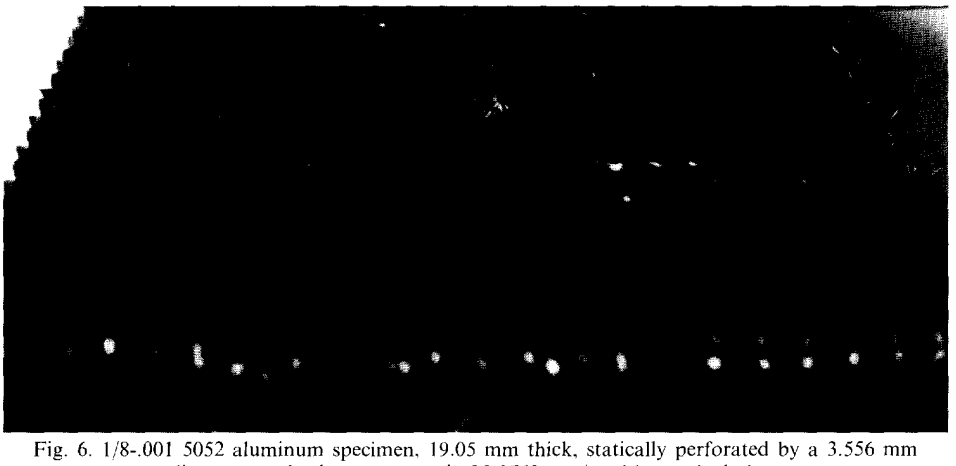

Fig. 6. 1/8-.001 5052 aluminum specimen, 19.05 mm thick, statically perforated by a 3.556 mm diameter steel sphere at a speed of 0.0762 mm/s, with attached plug.

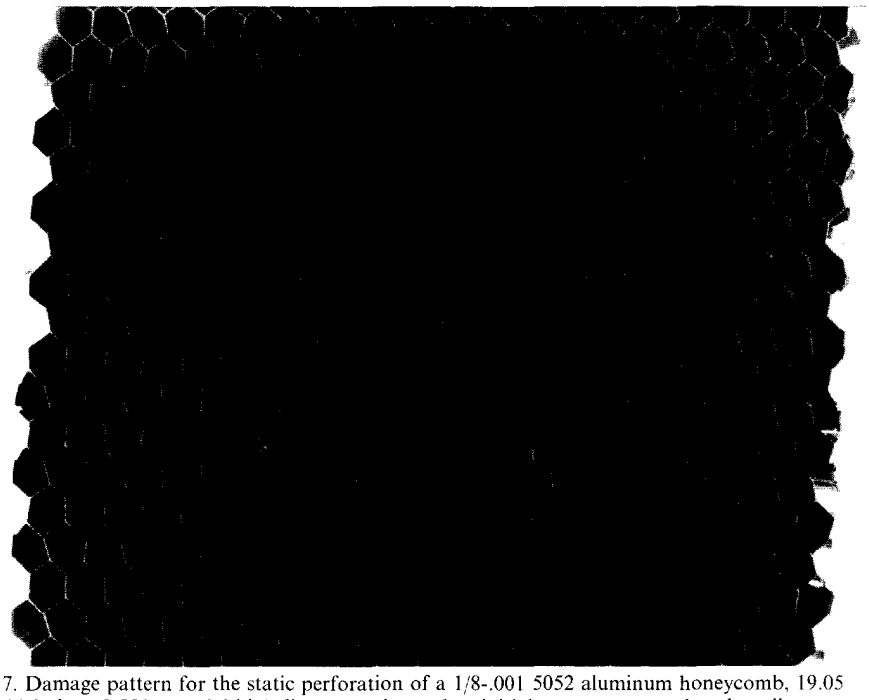

Fig. 7. Damage pattern for the static perforation of a 1/8-.001 5052 aluminum honeycomb, 19.05 mm thick, by a 3.556 mm (0.14 in) diameter sphere when initial contact occurred at the cell center (Run 21).

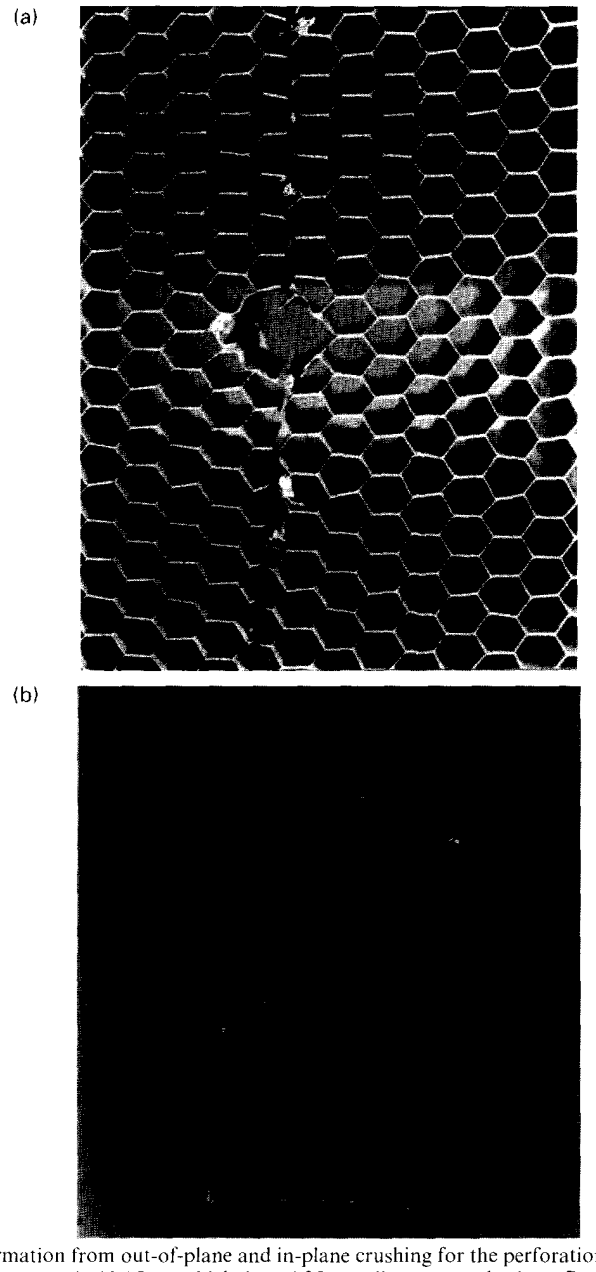

Fig. 9. Deformation from out-of-plane and in-plane crushing for the perforation of a 1/8-.001 5052 aluminum honeycomb, 19.05 mm thick, by a 6.35 mm diameter steel sphere. Perforation rate: 0.762 mm/s. Work of perforation: 4.15 Nm. (a) Plan view; (b) cross-section.

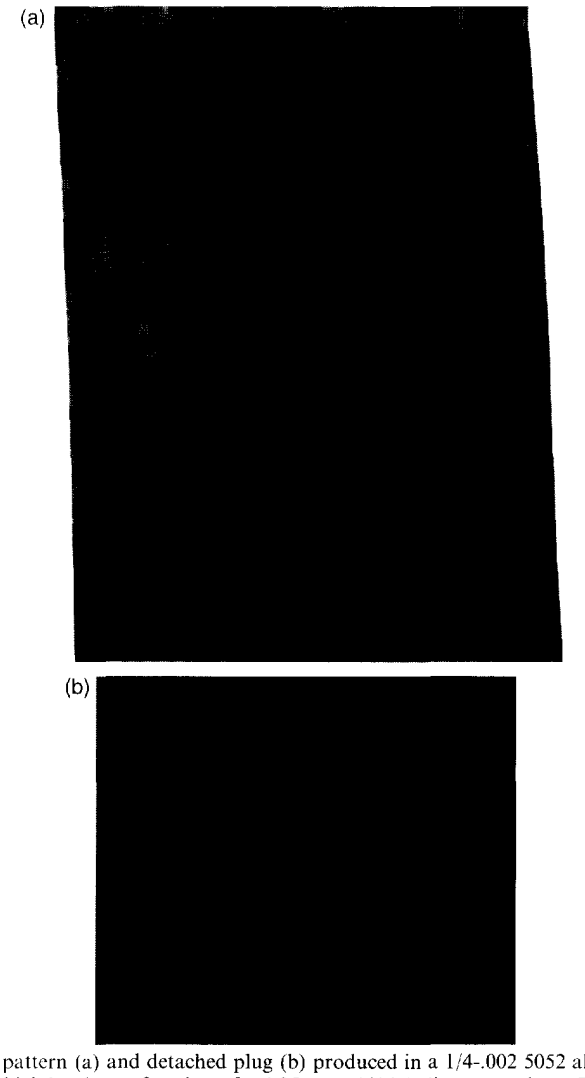

Fig. 11. Damage pattern (a) and detached plug (b) produced in a 1/4-.002 5052 aluminum honeycomb 19.05 mm thick by the perforation of a 6.35 mm (1/4 in) diameter sphere. Perforation rate: 0.0762 mm/s. Perforation work: 1.96 Nm.

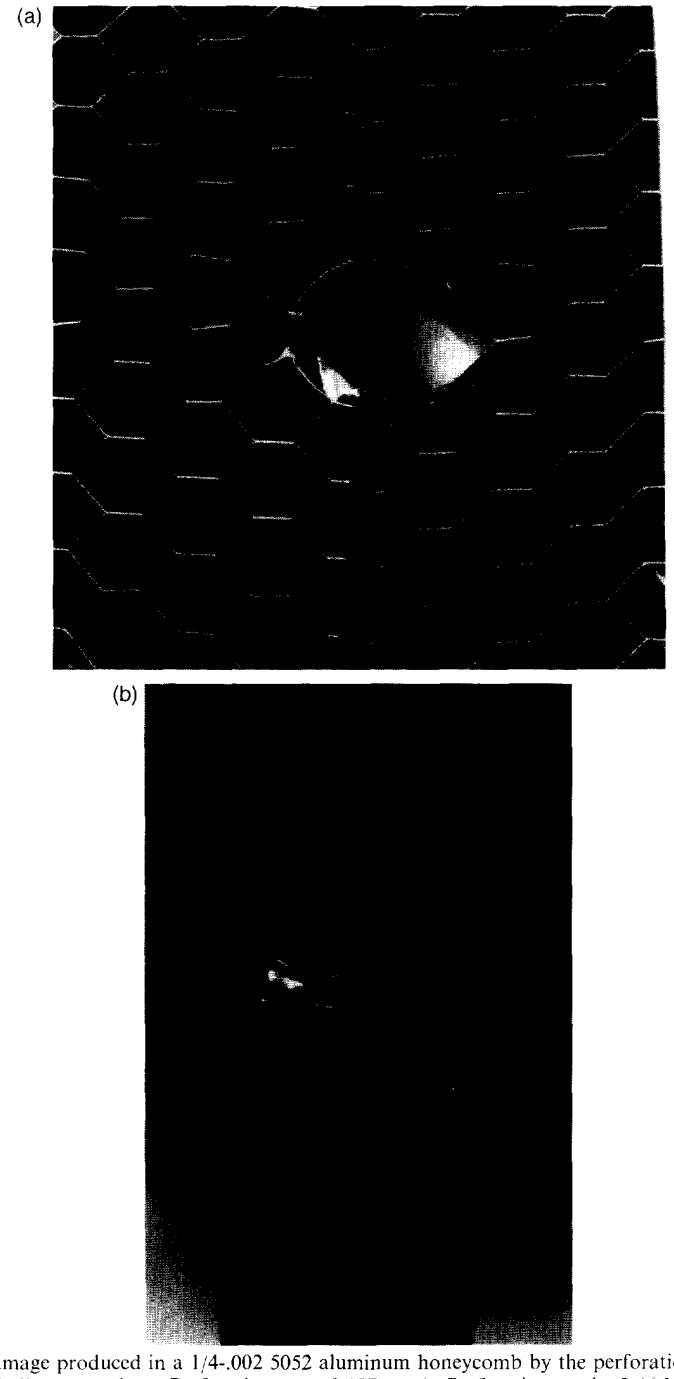

Fig. 12. Damage produced in a 1/4-.002 5052 aluminum honeycomb by the perforation of a 6.35 mm (1/4 in) diameter sphere. Perforation rate: 0.127 mm/s. Perforation work: 2.46 Nm. (a) Plan view; (b) cross-section.

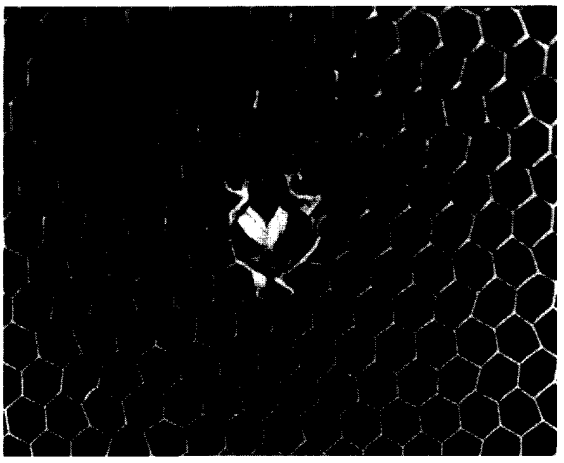

Fig. 16. Damage in a 1/8-.001 5052 aluminum honeycomb produced by a 6.35 mm diameter sphere striking with an initial velocity of 34.1 m/s. The projectile was arrested at the transition from out-of-plane to in-plane crushing.

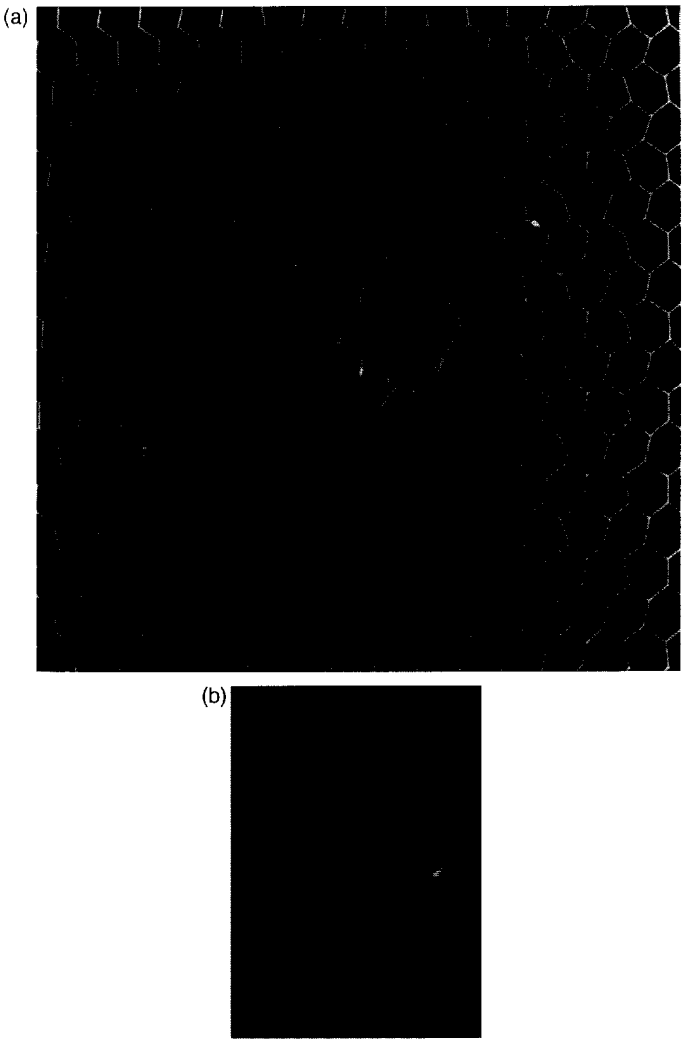

Fig. 17. Damage (a) including a separated plug (b) in a 1/8-.001 5052 aluminum honeycomb 19.05 mm thick perforated by a 6.35 mm diameter blunt cylinder at a velocity of 35.4 m/s.

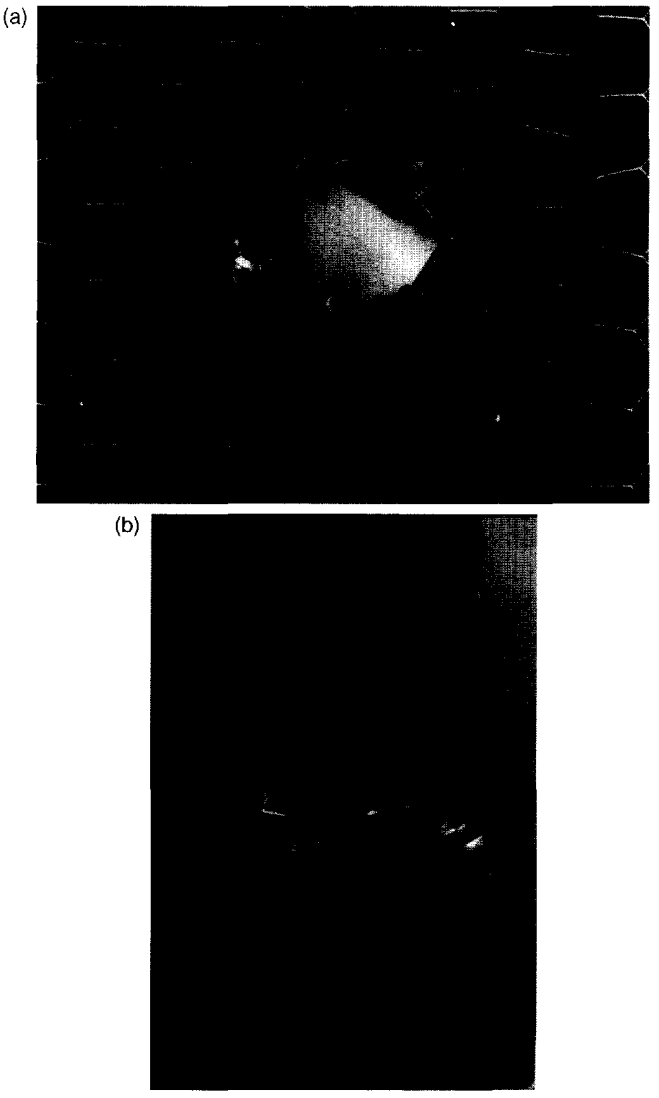

Fig. 18. Out-of-plane and in-plane crushing of a 1/4-.001 5052 aluminum honeycomb, 19.05 mm thick, by a 6.35 mm diameter sphere at a velocity of 78 m/s. (a) Plan view; (b) crushed region.

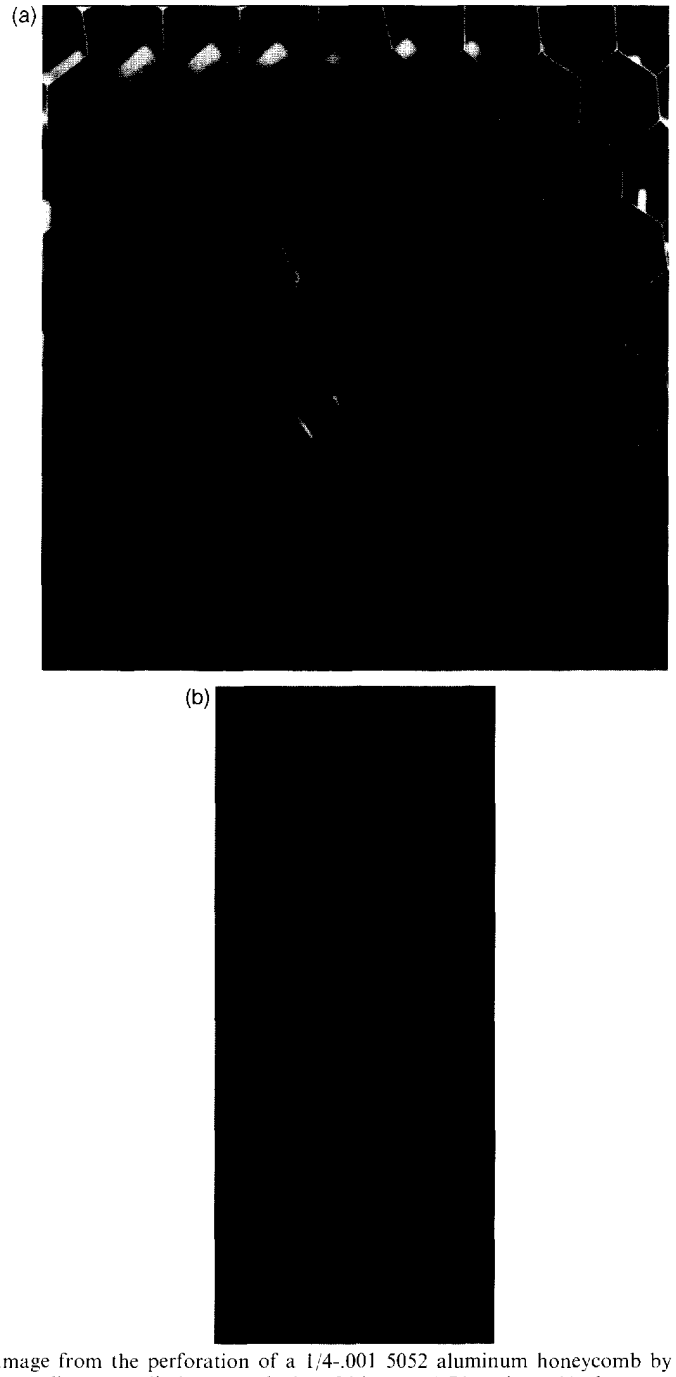

Fig. 19. Damage from the perforation of a 1/4-.001 5052 aluminum honeycomb by a 6.35 mm diameter cylinder at a velocity of 24 m/s. (a) Plan view; (b) plug.

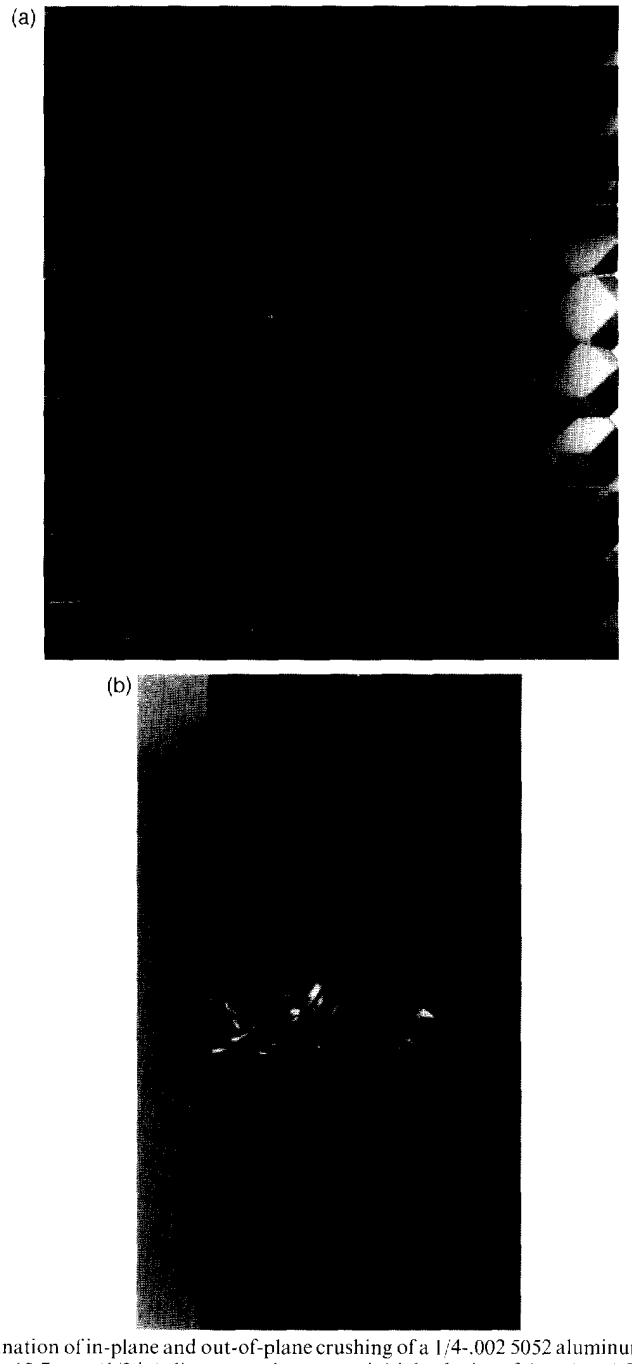

Fig. 20. Combination of in-plane and out-of-plane crushing of a 1/4-.002 5052 aluminum honeycomb perforated by a 12.7 mm (1/2 in) diameter sphere at an initial velocity of 65 m/s. (a) Plan view; (b) cross-section.

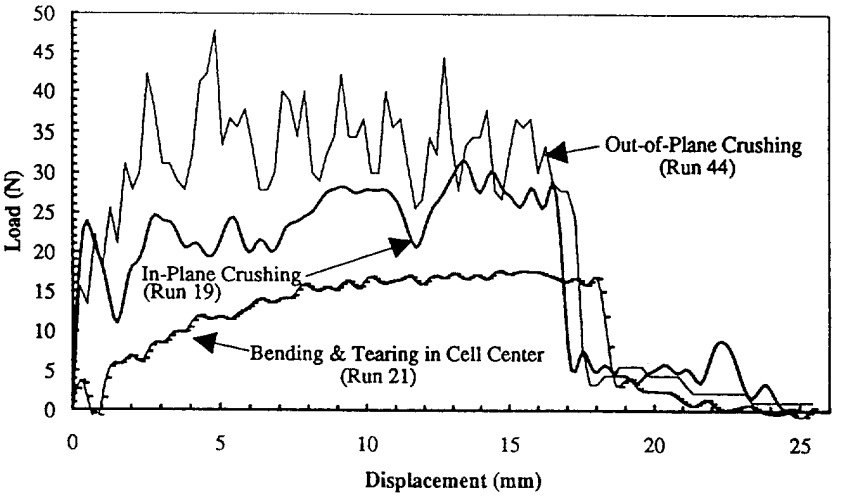

Fig. 8. Force–displacement curve for the static penetration of a 1/8-.001 5052 aluminum honeycomb 19.05 mm thick by a 3.556 mm diameter steel sphere in increasing amounts of energy absorption: Run 21: initial sphere placement in cell center. Principal damage mechanism is bending and tearing in cell center. Perforation rate: 0.127 mm/s. Perforation work: 0.257 Nm. Run 19: initial sphere placement over cell wall junction. Principal damage mechanism is in-plane crushing. Perforation rate: 0.127 mm/s. Perforation work: 0.443 Nm Run 44: initial sphere placement over cell wall. Principal damage mechanism is out-of-plane (axial) crushing. Perforation rate: 0.762 mm/s. Perforation work: 0.579 Nm.

number of cell walls. In two of these runs manifesting the least work of perforation, the penetration force returned to a null value at deformation depths of 10.2–12.7 mm, while the other two tests exhibited a very small, but measurable force value for the last third of the sample depth. The shape of the curve in Fig. 10, where a combination of perforation agents were active, differs substantially from those shown in Fig. 8, where, for each curve, a single mechanism was primarily responsible for the damage generated.

Run 33 also had a transition depth of 5.08 mm, but differed from the other four tests by exhibiting an immediate drop in load followed by a further increase in the penetration force above its transition value. This indicated that the in-plane crush load was greater than the axial crush value, which had not reached its full potential before the change to an in-plane damage pattern occurred. This run exhibited a different shape of the force–displacement curve, yielding a value of 0.680 J for the work of perforation. Run 32 produced

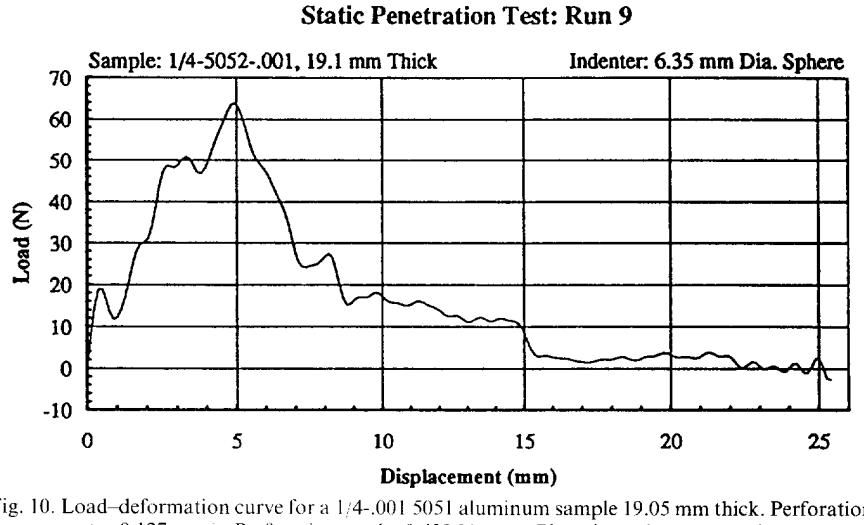

Fig. 10. Load–deformation curve for a 1/4-.001 5051 aluminum sample 19.05 mm thick. Perforation rate: 0.127 mm/s. Perforation work: 0.430 Nm. (a) Plan view; (b) cross-section.

a slightly greater depth of out-of-plane crush of 6.6 mm, but, as the sole exception for this series, a plug, which remained attached, was pushed through the sample ahead of the penetrator during the process of in-plane crushing. This also resulted in a much more irregularly-shaped load penetration curve which yielded the highest perforation energy of this series, 0.742 J.

For six corresponding tests with a 12.7 mm (1/2 in) diameter sphere, there was a similar correlation between the mechanism of deformation and the required work of perforation, ranging from 0.576–1.381 J. The two lowest energies of about 0.58 J were exerted when axial crushing was either non-existent or relatively small. Here, the walls distorted by the sphere were bent, delaminated and torn, permitting perforation without noticeable out-of-plane crushing. Run 25 exhibited a peak force of 89 N at a depth of 3.81 mm, while Run 2 manifested two peaks of 66.7 N at 5.08 and 9.14 mm, respectively; the shapes of these force curves were quite different both from each other and from the rest of the group.

With increasing depth of axial crush, up to a maximum of half the sample depth for the other runs of this group, the loading curves are approximately triangular. The peak forces, denoting the transition to transverse crushing, increase successively from 111 to 200 N; beyond the peak, the force diminishes rapidly with only nominal levels present during the later penetration process. The shape of these curves is similar to that shown in Fig. 10, albeit with about double the peak value. The absence of a plug for this series may be due to the large cell size and small foil thickness that produces greater in-plane flexibility, allowing an easier transition to in-plane crushing.

Six tests each were also performed on this material with a 0.002 in (0.051 mm) wall thickness for each of the two sizes of indenters, that were placed over the center of a wall or junction. For the smaller sphere, the two lowest energies of 1.215 and 1.526 J involved initial axial crush to a depth of 7.62 and 9.40 mm with peak forces of 178 N. At this point, the sphere slipped into the cell center and completed its passage solely by plastic bending of the wall. The other four runs involved axial followed by in-plane crushing and formation of plugs, all but one of which remained attached. The energy levels ranged from 1.839 to 2.522 J, transition occurring at approximately 10–11 mm with peak force levels ranging from 156 to 245 N, the latter for the highest penetration energies. The sample and the separated plug from Run 36 of this series are shown in Fig. 11.

When these targets were perforated by the 6.35 mm (1/2 in) diameter sphere, the resulting deformation modes were more uniform, involving axial crushing, plastic bending, delamination and tearing of the cell walls, but still subject to variations in the basically triangular load–displacement curve depending upon the depth when in-plane crushing initiated. Transition depths for Runs 4, 6, 28, 5, 29 and 30 were found to be 4.83, 5.84, 7.36, 6.86, 6.10 and 8.64 mm, respectively, with corresponding peak values of 311, 311, 356, 285, 311 and 400 N for an energy range of 2.282–3.490 J. The first two runs exhibited moderate drop rates with a secondary, smaller peak occurring in the declining force curve. Runs 5, 29 and 30 manifested a low force level during the final 3.8 mm of penetration. Figure 12 shows the head-on and section view of the damage due to sequential out-of-plane and in-plane crushing for Run 6, moving from left to right.

(*c*) *Comparison of results.* Table 2 summarizes the results of the static tests. Not surprisingly, for a given honeycomb size, the sphere with the larger projected area expends more work in perforation; with a specified indenter, a greater wall thickness exhibits the same trend. For the same foil thickness and indenter, the honeycomb with the smaller cell requires more perforation energy.

The predictions for the work of perforation from either primarily out-of-plane or primarily in-plane crushing determined from eqns (1) and (2) were compared with the perforation test data exhibiting primarily one or the other damage pattern. For the first type of crush, the flow stress was set equal to the ultimate tensile strength, according to Wierzbicki (1983), and obtained from the material properties presented in Table 1. Correspondence was unacceptable; however, the ratio of measured to calculated values for primarily out-of-plane crushing was substantially less, ranging from 1.5 to about 3, than

Table 2. Summary of static penetration test data on 5052 aluminum honeycomb

Honeycomb	Sphere diameter (mm)	Work (J)
1/8-.001	3.556	0.246–0.579
1/8-.001	6.35	0.709–1.486
1/8-.002	3.556	1.363–2.270
1/8-.002	6.35	3.351–5.186
1/4-.001	6.35	0.265–0.743
1/4-.001	12.7	0.576–1.381
1/4-.002	6.35	1.217–2.522
1/4-.002	12.7	2.282–3.490

the corresponding case for primarily in-plane crush damage, which produced a ratio of about 20. Thus, the neglected damage mechanisms are a relatively smaller energy consumption factor for axial crushing than for in-plane crushing.

A disagreement is expected in view of the neglect of the significant amount of energy required for the observed wall tearing. Both types of crush require this ripping to link the damaged to the virgin region of the sample. This tearing involves plastic deformation, ductile fracture and cell wall delamination. However, the discrepancy is so large that it was not considered appropriate to include the computed values of the perforation energy.

Another simplification, the assumption that tearing occurs at the edge of the indenter and that the crush area is the region directly in front of the sphere, requires modification, as the tearing occurred up to a wall length away from the perimeter. In such cases, the model underestimated the size of the crush area and hence that of the perforation work. It was found that changes in the locations of the tears led to slight variations in the average, out-of-plane crush load. In view of the apparent dominance of tearing and delamination, a more detailed modeling of this damage feature, probably requiring as its basis further detailed critical experimentation, appears to be required for a full description of these perforation processes.

(3) *Ballistic tests*

Damage patterns generated in the ballistic tests were virtually identical to those produced in the corresponding quasi-static tests.

(*a*) 3.175 *mm* (1/8 *in*) *cell size*

(*i*) *Thin-walled specimen* (0.001 *in*). Twenty-three tests using the 3.556 mm diameter sphere, 24 tests with the 6.35 mm diameter sphere, and 17 tests employing the cylinder were performed with the 1/8-0.001 aluminum honeycomb target. Curves of terminal velocity as a function of initial speed are presented in Figs 13–15 for the three projectiles which also show the value of the ballistic limit.

The location of the impact for the smaller diameter sphere again greatly affected the deformation modes. In the one instance when impingement occurred at the cell center, penetration proceeded by means of bending, tearing and delamination of walls, producing a slightly eccentric circular bore without significantly affecting adjacent elements. In all other cases of perforation, where a wall was impinged, the resulting damage depended on initial striker speed. Near the ballistic limit, the initial deformation consisted of either in-plane or out-of-plane crushing, followed upon lateral shifting of the sphere to the cell center by bending and tearing of the walls. This sequence of events is expected since, in this velocity range, the relatively small amount of energy of the striker is expended mostly in initial axial crushing.

When the projectile no longer has the capability for producing this type of damage, it will slip to the cell center where further penetration by bending and tearing requires less energy. With increasing impact speed, crushing extended to further depth. Half of the

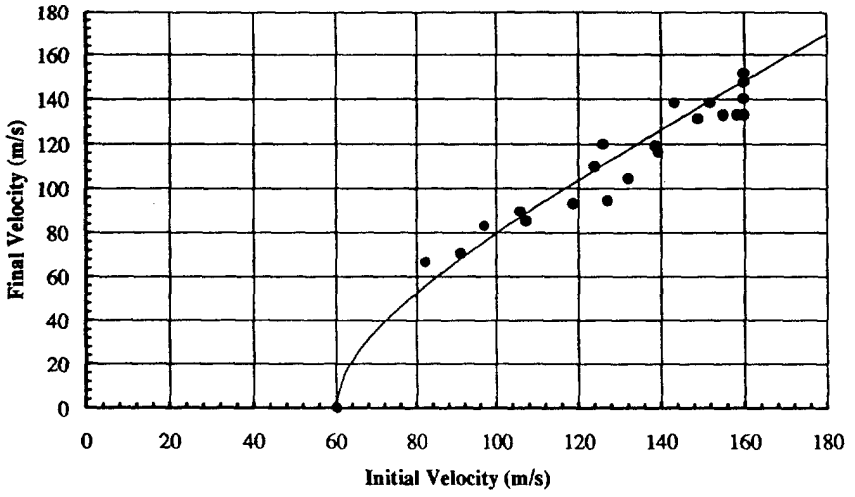

Fig. 13. Terminal vs initial velocity for a 3.556 mm diameter sphere perforating a 1/8-.001, 19.05 mm thick 5052 aluminum honeycomb.

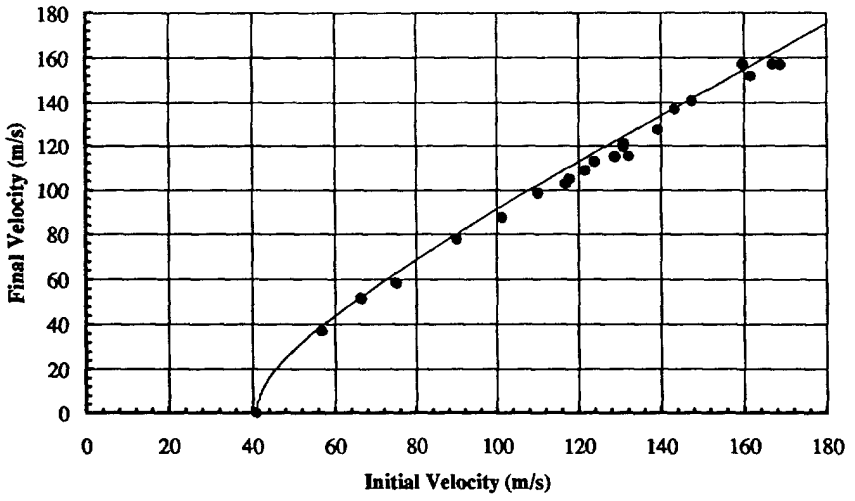

Fig. 14. Terminal vs initial velocity for a 6.35 mm diameter sphere perforating a 1/8-.001, 19.05 mm thick 5052 aluminum honeycomb.

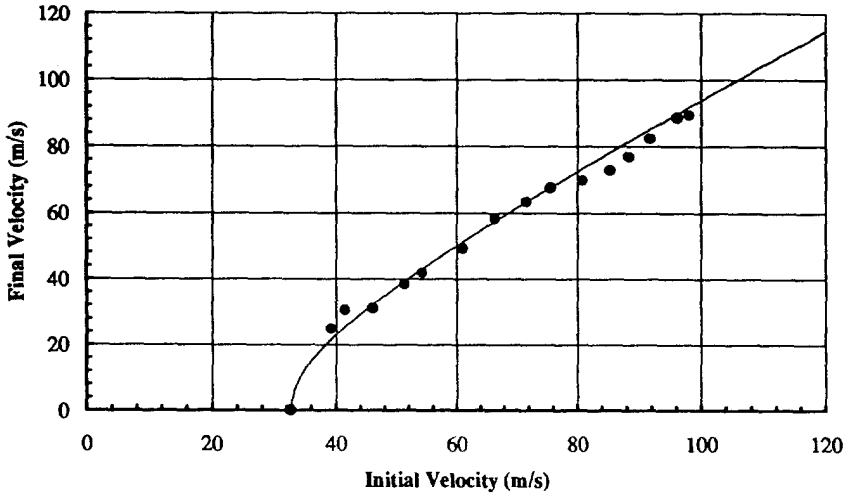

Fig. 15. Terminal vs initial velocity for a 6.35 mm diameter, 19.05 mm long blunt-faced steel cylinder perforating a 1/8-.001, 19.05 mm thick aluminum honeycomb.

perforated samples exhibited a combination of in-plane and out-of-plane crushing, while the other half displayed only in-plane crushing; none exhibited solely out-of-plane crushing and plug formation.

With the larger sphere, 15 (of 23) runs produced out-of-plane crushing with a tearing of only a portion of the walls linking the crushed to the virgin regions; this rotated the damage zone 90° and pushed it into the surrounding parts of the sample. The remainder of the perforation process occurred by in-plane crushing involving tearing of cell walls in front of the striker without plug formation. However, in one non-perforation case, the projectile was arrested at the transition from out-of-plane to in-plane deformation; the damage in this instance is portrayed in Fig. 16.

The 16 perforation runs with the cylinder at velocities ranging from 39 to 98 m/s exhibited only axial crushing due to the flat face presented to the target and an inability to move cell walls laterally. The sharp edge of the frontal surface produced efficient wall tearing, that formed a plug in every case. This occurred at a much lower force level than required for the sphere which, due to its rounded surface, could deform the cells both axially and laterally, but tore only a portion of the walls before the transition from out-of-plane to in-plane deformation. As exemplified in Fig. 17, the cylinders produced plugs shaped like elliptical pie pans with a central flat circular region constituting the bottom and the surrounding upward-folded material representing the side of the pan. The ratios of the major and minor diameter of the plug relative to that of the striker ranged from 1.68–2.42 and 1.52–2.23, respectively, while the ratio of overall plug to original sample thickness varied from 0.22–0.51. The masses of the plugs ranged from 0.0536–0.0791 g, the largest value being $\frac{1}{50}$th the mass of the striker.

(*ii*) *Thicker wall specimens* (0.002 *in*). Twenty tests using the 3.556 mm diameter sphere and 23 using the 6.35 mm diameter sphere were conducted. Most runs with the smaller sphere involved initial contact at a cell wall; at low velocities, an early in-plane or out-of-plane deformation occurred, followed by lateral motion of the striker to the cell center and completion of perforation by bending and delamination of the walls. When a sphere was initially positioned axially, only the latter mechanisms transpired, requiring less energy for perforation and producing a higher terminal velocity than a corresponding asymmetric impact at the same initial speed. As an example of this difference, a sphere with an initial speed of about 145 m/s striking the cell center exited with a speed of 114 m/s while that with the same original velocity impinging on a wall exhibited a terminal velocity of 78 m/s.

Half of the runs employing the larger sphere perforated solely by means of in-plane crushing, while the other half started with out-of-plane crushing and subsequently changed to an in-plane deformation mode. No specimen exhibited purely axial crushing or plug formation.

(*b*) 1/4 (6.35 *mm*) *cell size*

(*i*) *Thin-walled specimens* (0.001 *in*).Twenty-nine runs were conducted with the 6.35 mm diameter sphere; only one initially struck the cell center effecting perforation by bending of cell walls. In six of the other tests, with an impact speed near the ballistic limit of 36.6 m/s, the sphere slipped into the cell center after initial axial crushing. The rest of the test set featured either combined out-of-plane and in-plane, or else only in-plane crushing, without generating a plug. A typical damage pattern for this combination is shown in Fig. 5.

The ballistic limit of this honeycomb for the larger sphere was 16.8 m/s. Samples for most runs exhibited initial out-of-plane crushing which transformed to in-plane crushing after partial penetration, as illustrated in Fig. 18, where the section view depicts the axially crushed cell walls. Only three runs manifested in-plane crushing throughout the entire perforation process. No plugs were formed as the curved surface of the sphere experienced difficulty in tearing cell walls at the perimeter, and the thin wall and large cell diameter

provide for flexible in-plane deformation. Thus, the striker experienced no difficulty in rotating the axially crushed material and completing the perforation with in-plane crushing.

As was the case for the smaller cell size, cylinder perforation, with a ballistic limit of 23.6 m/s, proceeded primarily by axial crushing and plug formation, as shown in Fig. 19. The plug, shaped here also like a pie pan, exhibited a range of ratios of major and minor diameters to striker diameters of 1.24–2.70 and 1.16–2.49, respectively, a ratio of plug to initial specimen thickness range of 0.15–0.69, and a plug mass ranging from 0.02–0.081 g, compared to a striker mass of 4.66 g.

(*ii*) *Thick-walled specimens* (0.002 *in*). Twenty-three tests were conducted on this type of specimen with the 6.35 mm (1/4 in) diameter sphere, and 21 runs were executed with the 12.7 mm (1/2 in) diameter sphere. Only four of the tests with the smaller sphere struck at the cell center causing bending and delamination of the walls during perforation. In other runs at lower initial velocities, the striker impinged on a wall and, after initial penetration, rapidly moved to the cell center, changing its damage pattern from axial crush to wall flexure and separation.

In comparison to (i) of this series, the sphere here displayed a greater tendency to change lateral position. Runs at higher initial velocity generally featured either a combination of out-of-plane and in-plane crushing, or solely in-plane crushing throughout. None of the tests produced axial crushing and plug formation, in contrast to the corresponding static case where most of the samples formed a plug. A possible explanation for this discrepancy is the greater lateral constraint present in the static tests, whereas ballistic loading permitted greater in-plane motion of the striker.

As with the other series, damage generated by the 12.7 mm diameter sphere consisted of in-plane crushing throughout or a combination of this mechanism and out-of-plane crushing. The latter case is exemplified in Fig. 20.

Damage details for all static and dynamic runs may be found in Louie (1992).

(4) *Ballistic limits*

Table 3 presents the measured ballistic limits, constituting the average of the highest non-perforation and lowest perforation speeds. A calculation of this limit by equating the kinetic energy to relations (1) and/or (2) proved to be unsatisfactory, often underpredicting the value by factors of up to eight for in-plane deformation. The values for out-of-plane crushing were somewhat closer, but are also not listed. However, in cases where the damage consisted of substantial portions of both in-plane and out-of-plane crushing, the predictions using only the out-of-plane mode, eqn (1), were reasonably close, as may be noted from the footnote to Table 3. The reasons for the other discrepancies, identical to those discussed

Table 3. Summary of measured ballistic limits for 5052 aluminum honeycomb 19.05 mm thick

Honeycomb		Projectile			
Type	Areal density (kg/m^2)	Type	Mass ($kg \times 10^{-3}$)	Primary deformation mode†	Measured ballistic limit (m/s)
1/8-.001	1.37	3.556 mm *D* sphere	0.186	IC	60.4
1/8-.001	1.37	6.35 mm *D* sphere	1.04	IC	40.8
1/8-.001	1.37	6.35 mm *D*, 19.05 mm long cylinder	4.66	OC	32.6
1/8-.002	2.47	3.556 mm *D* sphere	0.186	IC	120
1/8-.002	2.47	6.35 mm *D* sphere	1.04	IC	73.2
1/4-.001	0.70	6.35 mm *D* sphere	1.04	IC	36
1/4-.001	0.70	12.7 mm *D* sphere	8.35	OC/IC[1]	16.9
1/4-.001	0.70	6.35 mm *D*, 19.05 mm long cylinder	4.66	OC	23.6
1/4-.002	1.27	6.35 mm *D* sphere	1.04	OC	44.8
1/4-.002	1.27	12.7 mm *D* sphere	8.05	OC/IC[2]	24.6

† IC = in-plane crushing; OC = out-of-plane crushing.
[1] Calculated ballistic limit for OC: 14.6 m/s; [2]Calculated ballistic limit for OC: 25.8 m/s.

previously for the static work of perforation, involve the neglect of significant damage mechanisms.

The determination of the actual crush area for a valid analytical model (rather than projected area of the striker) is illustrated by the following example. An upper bound of the crush area may be taken as the face of the elliptical plug produced by the cylinder striking the 1/8-.001 honeycomb at the ballistic limit, amounting to 107 mm^2. On the other hand, the frontal face of the cylinder had an area of only 31.6 mm^2; when the value of the maximum plug area is used, the calculated ballistic limit (from the out-of-plane crushing expression) differs negligibly from the observed value. The correct average value of the crushed area lies somewhat between the upper bound cited and the projected area.

The results shown in Table 3 for the 12.7 mm diameter sphere involve samples clamped between face plates, while the others pertain solely to specimens clamped at two opposite edges. It is interesting to observe that the deformation patterns for the edge-clamped honeycombs were either completely in-plane or out-of-plane, whereas the fully clamped samples exhibited a combination of both, perhaps due to the enforced suppression of greater global deformations.

The data also verified the intuitive fact that, for a given size of honeycomb, the projectile with the smaller mass exhibits a higher ballistic limit, but not in proportion to the mass of the penetrators. Similarly, for a given cell size and striker, the honeycomb with the thicker foil displayed a higher ballistic limit, but in a ratio somewhat less than that of the wall thickness. Again, as expected *a priori*, the honeycomb with the smaller cell size produces a higher limit for the same wall thickness and striker geometry.

No data are available for the ballistic limit of the projectiles for solid aluminum plates of the same, or even nearly the same areal density as the honeycombs listed in Table 3. The nearest measured values were obtained for 2024-0 or 2024-T3 aluminum 1.27 mm thick, constituting an areal density of 3.40 kg/m^2 [see e.g. Calder and Goldsmith (1971), Goldsmith and Finnegan (1971)]. The plates were variously supported, but no significant global deformations were observed. The ballistic limit for the 6.35 mm diameter sphere was determined to be 170 m/s and that for the 12.7 mm diameter sphere was 130 m/s. These values are nearly twice that obtained for the 1/8-.002 and 1/4-.002 honeycombs, even when the limits for the cellular targets were adjusted by the ratio of their respective densities. The only ballistic limit data for this thickness of aluminum plate pertains to the impact of a 12.7 mm diameter, 19.07 mm long blunt-nosed cylinder with a mass of 39.5 g where a speed of 54.2 m/s was measured. No correlation can be expected for this striker with the results presented in Table 3.

(5) *Comparison of static and dynamic perforation work*

The expressions cited for calculating damage, which do not accurately predict the work of penetration and the ballistic limit because of the neglect of significant energy losses also do not distinguish between static and dynamic perforation. However, both the manufacturer [Hexcel Corporation (1988)] and previous investigations [see e.g. Goldsmith and Sackman (1992)] indicated that the dynamic crush strength of aluminum honeycomb ranged up to 50% greater than the static value, attributed to strain rate effects. Table 4 presents a comparison for similar modes of deformation of the static and dynamic (at the ballistic limit) work of perforation where data were obtained; data for dissimilar damage patterns for the two types of loading are not presented. Ballistic tests tend to produce in-plane crushing, while static tests most frequently exhibit out-of-plane crushing. In the four cases where the comparison of loading rates could be accomplished, there was insufficient evidence of any trend indicating augmented work under dynamic conditions. It is possible that the effect of an increased yield or fracture limit at higher loading rates is counter-balanced by a lower required energy for some of the other mechanisms involved in the perforation process, such as delamination.

It is also interesting to note that a doubling of the cell wall for the 1/8 in diameter cell requires approximately a fourfold amount of energy for perforation, whereas the energy is only doubled for the larger 1/4 in cell diameter. It is presumed that this situation prevails because, in the first case, there is less space into which the deformed wall material can

Table 4. Static and dynamic (ballistic limit) work of axial perforation for 5052 aluminum honeycomb 19.05 mm thick

Honeycomb	Projectile	Projectile mass (g)	Principal deformation mode	Work (J) Static	Work (J) Dynamic
1/8-.001	3.556 mm *D* sphere	0.186	IC†	0.338	—
1/8-.001	6.35 mm *D* sphere	1.04	IC	0.873	0.811
1/8-.001	6.35 mm *D*, 19.05 mm long cylinder	4.66	OC‡	2.475	—
1/8-.002	3.556 mm *D* sphere	0.186	IC	1.333	—
1/8-.002	6.35 mm *D* sphere	1.04	IC	2.791	—
1/4-.001	6.35 mm *D* sphere	1.04	IC	0.672	—
1/4-.001	12.7 mm *D* sphere	8.35	OC/IC	1.187	0.575–1.380
1/4-.001	6.35 mm *D*, 19.05 mm long cylinder	4.66	OC	1.300	—
1/4-.002	6.35 mm *D* sphere	1.04	OC	1.049	1.216
1/4-.002	12.7 mm *D* sphere	8.35	OC/IC	2.531	2.280–3.487

† IC = In-plane crushing.
‡ OC = Out-of-plane crushing.

expand and thus additional work needs to be performed in order to accommodate the displaced aluminum.

(6) *Comparison of final velocities*

The terminal velocities observed in selected projectile/target combinations are shown as points in Figs 13–15. These graphs are typical of the results of other projectile/target combinations. Any attempt to compare these data with results from eqn (2) using the predicted perforation work is bound to show massive discrepancies in view of the known disparity in the calculated and measured work of static and dynamic perforation. In consequence, the prediction, eqn (3), shown as the solid line in these figures, utilized the measured value of the ballistic limit work, shown in Table 4, rather than any theoretical equivalent. This procedure follows the commonly adopted concept that this limit is generally considered to be a property of the system (material and geometry) and thus can properly be derived from experiments. The plug mass, when present, was chosen as the average value from the test results. The comparison is thus not based on totally independent approaches, but does indicate good correlation when the actual work of perforation as represented by the ballistic limit is more precisely determined and the plug mass is properly ascertained.

The reasonable correspondence between the curve and the data points at higher initial velocities should be noted since the types of deformation there are quite different from those at the ballistic limit. The reason for this accord is the fact that the work required to just perforate the sample becomes an increasingly smaller fraction of the total energy, so that the computed final velocity is not significantly affected. The greatest deviation occurs just above the ballistic limit when changes in deformation mechanisms take place at only slightly higher initial velocities, as exemplified by Fig. 21.

It should be reemphasized that if the projectile diameter is equal to the cell size, numerous modes of deformation can occur, usually depending on the precise impact point, and leading to significant variations in the final velocity for a fixed impact speed slightly above the ballistic limit. When the striker diameter is twice the cell size, the deformation mechanisms are less numerous, and the range of final velocities is smaller for identical initial conditions, leading to less scatter. This feature is demonstrated by a comparison of Figs 13 and 14.

Ballistic tests with the cylinder using witness screens for the final velocity determination revealed that the projectile tends to tumble. However, calculations for a typical run indicated that the energy transformed to this type of rotation constituted less than 2% of the translational kinetic energy and thus would not affect the calculated results.

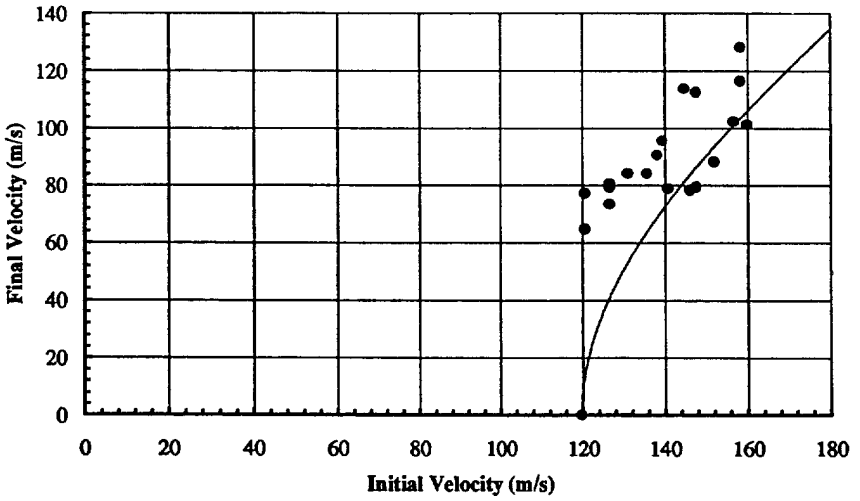

Fig. 21. Terminal vs initial velocity for a 3.556 mm diameter sphere perforating a 1/8-.002, 19.05 mm thick 5052 aluminum honeycomb.

CONCLUSION

An experimental study of the axial perforation of two aluminum honeycombs with cell diameters of 3.175 mm (1/8 in) and 6.35 mm (1/4) in and wall thicknesses of 1 and 2 mils (0.025–0.051 mm) by two steel spheres of the same or double the cell size, was conducted under both quasi-static and ballistic conditions. The sample thickness was maintained constant at 19.05 mm (3/4 in). Dynamic tests on these samples were also performed using a cylinder with a diameter of 6.35 mm and an L/D ratio of 3. Detailed descriptions of the manifestation of the major energy absorbing mechanisms are presented, although it was not possible to provide a global characterization that uniquely linked initial conditions to the phenomena observed. This also has prevented the development of a reasonably accurate phenomenological model at this stage.

Major modes of deformation consisted of out-of-plane or in-plane crushing, with the former manifesting substantially greater tearing and delamination of walls and a resulting substantially larger energy expenditure. Transition from out-of-plane to in-plane crushing was indicated by a noticeable drop in the perforation force. Quasi-static penetration exhibited a greater variety of damage mechanisms than ballistic impact; for example, plugs were formed in some cases by very slow penetration of spheres, whereas this was produced only by the flat-faced cylinder under ballistic conditions.

In case of the spheres, the principal damage mechanism manifested in both types of test was critically dependent on the position of initial contact when their diameter approximated that of the cell size. When contact occurred at the center of a wall or at a junction of cells, initial penetration involved out-of-plane crush, which was transformed to in-plane crushing after the sphere moved laterally to a position at or near the cell center. When the penetrator diameter was twice the cell size, this feature was not so critical. All cylinder tests involved only axial crushing and the production of a plug.

In the static tests, the largest amount of energy was consumed for the 1/8-.002 sample which featured bending without tearing. All other conditions being equal, the sphere with the larger projected area, or the sample with the thicker wall, or the honeycomb with the smaller cell size required a greater amount of perforation energy than the converse.

Dynamic tests generally exhibited a similar damage pattern. For equal cell and sphere diameters, central impact produced bending, tearing and delamination of one cell only, and damage did not spread to adjacent cells. Near the ballistic limit of the spheres, initial out-of-plane crushing shifts to in-plane crushing by bending and tearing of cell walls; at higher initial velocities, out-of-plane extends further into the specimen. This is the sole mechanism for perforation by cylinders which uniformly generate a dish-shaped plug and requires less energy for this action than perforation by spheres.

Since the penetration and perforation behavior of the honeycombs near the ballistic limit was frequently found to be random, previously developed expressions for axial and in-plane crushing did not provide an accurate prediction of the energy absorbed during such processes. These models neglect the tearing and delamination of the cell walls which dominate in-plane crushing and which also appear to significantly influence out-of-plane deformation. In general, a sound prediction of the ballistic limits fails for similar reasons. However, when the experimental ballistic limit is used as a system property, as is common practice, the measured terminal velocity is in good accord with the predicted value, particularly as the impact speed is raised well beyond the value of the ballistic limit. Furthermore, the details of the cellular deformations will become increasingly less critical in this range.

Acknowledgment—The authors would like to express their appreciation to Hexcel Corporation, Dublin, CA, and, in particular, to Mr Tom Bitzer, for the donation of honeycomb samples. A portion of this work was abstracted from the thesis of the second author, submitted to the University of California, Berkeley, in partial fulfilment of the M.S. degree requirement.

REFERENCES

Backman, M. E. and Goldsmith, W. (1978). The mechanics of penetration of projectiles into targets. *Int. J. Engng Sci.* **16,** 1–99.

Calder, C. A. and Goldsmith, W. (1971). Plastic deformation and perforation of thin plates resulting from projectile impact. *Int. J. Solids Structures* **7,** 863–881.

Gibson, L. J. and Ashby, M. F. (1988). *Cellular Solids, Structure and Properties*. Pergamon Press, Oxford

Goldsmith, W. and Finnegan, S. A. (1971). Penetration and perforation processes in metal targets at and above ballistic velocities. *Int. J. Mech. Sci.* **13,** 843–866.

Goldsmith, W. and Sackman, J. L. (1992). An experimental study of energy absorption in impact on sandwich plates. *Int. J. Impact Engng* **12,** 241–262.

Hexcel Corporation, Dublin, CA (1988). Mechanical Properties of Hexcel Honeycomb Materials. TSB 120.

Jamjian, M., Sackman, J. L. and Goldsmith, W. (1994). Response of an infinite plate on a honeycomb foundation to a rigid cylindrical impactor. *Int. J. Impact Engng.* **15,** 183–200.

Jenq, S. T. and Goldsmith W. (1988). Effect of target bending in normal impact of a flat-ended cylindrical projectile near the ballistic limit. *Int. J. Solids Structures* **24,** 1243–1266.

Klintworth, J., W., and Stronge, W. J. (1988). Elasto–plastic yield limits and deformation laws for transversely crushed honeycombs. *Int. J. Mech. Sci.* **30,** 273–292.

Klintworth, J. W., and Stronge, W. J. (1989). Plane punch indentation of a ductile honeycomb. *Int. J. Mech. Sci.* **31,** 359–378.

Landkof, B., and Goldsmith, W. (1985). Petalling of thin, metallic plates during penetration by cylindro-conical projectiles. *Int. J. Solids Structures* **21,** 245–266.

Liss, J., and Goldsmith W. (1984). Plate perforation phenomena due to normal impact by blunt cylinders. *Int. J. Impact Engng* **2,** 37–64.

Liss, J., Goldsmith, W., and Kelly, J. M. (1983) A phenomenological penetration model of plates. *Int. J. Impact Engng* **1,** 321–341.

Louie, Dell L. (1992). Static Penetration and Ballistic Limits of Aluminum Honeycomb. Thesis (M.S.), University of California, Berkeley.

Moriarty, K. and Goldsmith, W. (1993). Dynamic energy absorption characteristics of sandwich shells. *Int. J. Impact Engng* **13**(2) 293–317.

Recht, R. F. and Ipson, T. W. (1963). Ballistic perforation dynamics. *J. Appl. Mech.* **30,** 384–390.

Taylor, G. I. (1948). The formation and enlargement of a circular hole in a thin plastic sheet. *Quart. J. Mech. Appl. Math.* **1**(1), 103–124.

Thomsen, W. T. (1955). An approximate theory of armor penetration, *J. Appl. Phys.* **26,** (1983). 80–82.

Wierzbicki, T. (1983). Crushing analysis of metal honeycombs. *Int. J. Impact Engng* **1** 157–174 (1989).

Zhang, J. and Ashby, M. F. (1989). Energy absorption of foams and honeycombs. Cambridge Univ. Engineering Department, CUED/C-MATS/TR 159.

Zhang, J. and Ashby, M. F. (1992a). The out-of-plane properties of honeycombs. *Int. J. Mech. Sci.* **34,** 475–489.

Zhang, J., and Ashby, M. F. (1992b). Buckling of honeycombs under in-plane biaxial stresses. *Int. J. Mech. Sci.* **34,** 491–509.